

# Make RepVGG Greater Again: A Quantization-aware Approach

Xiangxiang Chu Liang Li Bo Zhang  
Meituan

chuxiangxiang, liliang58, zhangbo97@meituan.com

## Abstract

The tradeoff between performance and inference speed is critical for practical applications. Architecture reparameterization obtains better tradeoffs and it is becoming an increasingly popular ingredient in modern convolutional neural networks. Nonetheless, its quantization performance is usually too poor to deploy (e.g. more than 20% top-1 accuracy drop on ImageNet) when INT8 inference is desired. In this paper, we dive into the underlying mechanism of this failure, where the original design inevitably enlarges quantization error. We propose a simple, robust, and effective remedy to have a quantization-friendly structure that also enjoys reparameterization benefits. Our method greatly bridges the gap between INT8 and FP32 accuracy for RepVGG. Without bells and whistles, the top-1 accuracy drop on ImageNet is reduced within 2% by standard post-training quantization.

## 1. Introduction

Albeit the great success of deep neural networks in vision [4, 12, 17, 19, 35], language [6, 40] and speech [13], *model compression* has become more than necessary, especially considering the paramount growth of power consumption in data centers, and the voluminous distribution of resource-constrained edge devices worldwide. Network quantization [14, 15] is one of the most proficient approaches because of the lower memory cost and inherent integer computing advantage.

Still, quantization awareness in neural architectural design has not been the priority and has thus been largely neglected. However, it may become detrimental where quantization is a mandatory operation for final deployment. For example, many well-known architectures have quantization collapse issues like MobileNet [20, 21, 36] and EfficientNet [38], which calls for remedy designs or advanced quantization schemes like [26, 37, 45] and [2, 16] respectively.

Lately, one of the most influential directions in neural architecture design has been reparameterization [8, 11, 46]. Among them, RepVGG [11] refashions the standard Conv-

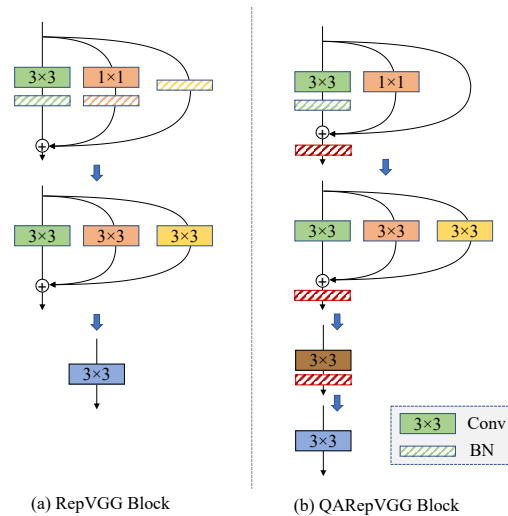


Figure 1. Reparameterization of QARepVGG block compared with RepVGG block. Both can be identically fused into a single Conv  $3 \times 3$  but QARepVGG is quantization-friendly to have 70.4% after PTQ while RepVGG drops to 52.2% [7].

BN-ReLU into its identical multi-branch counterpart during training, which brings powerful performance improvement while adding no extra cost at inference. For its simplicity and inference advantage, it is favored by many recent vision tasks [10, 22, 28, 39, 41, 44]. However, reparameterization-based models face a well-known *quantization difficulty* which is an intrinsic defect that stalls industry application. It turns out to be non-trivial to make this structure comfortably quantized. A standard post-training quantization scheme tremendously degrades the accuracy of RepVGG-A0 from 72.4% to 52.2%. Meantime, it is not straightforward to apply quantization-aware training [7].

Here, we particularly focus on the quantization difficulty of RepVGG [11]. To resolve this problem, we explore the fundamental quantization principles that guide us through in-depth analysis of the typical reparameterization-based architecture. That is, for a network to have better quantization performance, the distribution of weights as well as the

processed data of an arbitrary distribution shall be quantization friendly. Both are crucial to ensure better quantization performance. More importantly, these principles lead us to a brand new design which we call QARepVGG (short for Quantization-Aware RepVGG) that doesn't suffer from substantial quantization collapse, whose building block is shown in Fig. 1 and its quantized performance has been largely improved.

Our contributions are threefold,

1. Unveiling the root cause of performance collapse in the quantization of the reparameterization-based architecture like RepVGG [11].
2. Contriving a quantization-friendly replacement (*i.e.* QARepVGG) of RepVGG which holds fundamental differences in terms of weight and activation distribution, meanwhile preserving the very advantage of outstanding speed and performance trade-off.
3. Our proposed method generalizes well at different model scales and on various vision tasks, achieving outstanding post-quantization performance that is ready to deploy. Besides, our models are comparable to RepVGG in terms of FP32 accuracy.

Expectedly, our approach will greatly boost the quantized performance with no extra cost at inference, bridging the gap of the last kilometer during the deployment of reparameterized networks. We will release the code to facilitate reproduction and future research.

## 2. Related Work

**Reparameterization Architecture Design.** RepVGG [11] leverages an over-parameterized network in the form of multiple branches at the training stage and identically fuses branches into one during inference, which is known as reparameterization. The follow-up works DBBNet [9] and MobileOne [39] extend this design by introducing diversified compositions, enhancing the trade-off between performance and latency. This reparameterization trend also applies to recent object detection methods like PPYOLO-E [44], YOLOv6 [28] and YOLOv7 [41].

**Quantization.** *Network Quantization* is an effective model compression method that maps the network weights and input data into lower precisions (typically 8-bit) for fast calculations, which greatly reduces the model size and computation cost. Without compromising much performance, quantization is mostly adopted to boost speed before deployment, serving as a de facto standard in industrial production. Post-Training Quantization (PTQ) is the most common scheme as it only needs a few batches of images to calibrate the quantization parameters and it comes with no extra training. Quantization-Aware Training (QAT)

methods have also been proposed to improve the quantized accuracy, such as integer-arithmetic-only quantization [24], data-free quantization [32], hardware-aware quantization [42], mixed precision quantization [43], zero-shot quantization [3]. As QAT typically involves intrusion into the training code and requires extra cost, it is only used when the training code is at hand and PTQ can't produce a satisfactory result. To best showcase the proposed quantization-aware architecture, we mainly evaluate the quantized accuracy using PTQ. Meanwhile, we include experiments to demonstrate it is also beneficial for QAT.

**Quantization-aware architecture design.** A quantization-friendly replacement of separable convolution is proposed in [37], where a metric called signal-to-quantization-noise ratio (SQNR) is defined to diagnose the quantization loss of each component of the network. It is also argued that weights shall obey a uniform distribution to facilitate quantization [37]. Swish-like activations are known to have quantization collapse which either requires a delicate learnable quantization scheme to recover [2], or to be replaced by RELU6 as in EfficientNet-Lite [30]. BatchQuant [1] utilizes one-shot neural architecture search for robust mixed-precision models without retraining.

**Quantization for Reparameterization Network.** It is known that reparameterization-based architectures have quantization difficulty due to the increased dynamic numerical range due to its intrinsic multi-branch design [7]. The accuracy degradation of reparameterization models via PTQ is unacceptable. Since the reparameterized network in deploy mode lacks the BN layer, it is difficult to improve the quantization accuracy using QAT [7]. To our best knowledge, RepOpt-VGG [7] is the only related work that makes an effort to resolve this quantization issue by crafting a two-stage optimization pipeline. RepOpt-VGG claims that the quantization difficulty is caused by the quantization-unfriendly parameter distribution of the fused kernels. We reinvestigate this problem to discover that it is far more complicated and the huge quantization error is a result of the collaborative effect of weights and activation.

## 3. Make Reparameterization Quantization Friendly

Several sources might introduce errors in a standard quantization pipeline [37]. We select *mean square error* (MSE) as the metric following [16] to measure the quantization error for a tensor,

$$MSE(Q(\mathbf{w}, t, n_b), \mathbf{w}) = \frac{1}{n} \sum_i (Q(\mathbf{w}_i, t, n_b) - \mathbf{w})^2. \quad (1)$$

where  $Q$  is the quantization process,  $\mathbf{w} \in \mathbb{R}^n$  the weights of  $n$  channels, a clamping threshold  $t$  and  $n_b$  the bit-width. The specific quantization error is determined by several

factors of the tensor distribution, including the *maximum and minimum values*, *standard deviation*, and the *clamping threshold*, etc. Unfortunately, we can not give a concrete solution since we can not hypothesize any distribution for tensors in a network. In practice, we consider a quantization-friendly distribution as one that has relatively a small numerical range and a small standard deviation.

As for a reparameterization-based architecture, there are two main components, weight and activation, that require quantization and may lead to accuracy degradation. Activation also serves as the input of the next layer, so the errors are incremented layer by layer. Therefore, good quantization performance for neural networks requires mainly two fundamental conditions:

- C1** weight distribution is advantageous for quantization,
- C2** activation distribution (*i.e.* how the model responds to input features) is tractable for quantization.

Empirically, violating either one of them will lead to inferior quantization performance. We use RepVGG-A0 as an example to study why the quantization of the reparameterization-based structure is difficult.

### 3.1. Diving into the Quantization Failure of Reparameterization Structure

We first reproduce the performance of RepVGG-A0 with its officially released code [7], shown in Table 1. Based on this, we can further strictly control the experiment settings. We quantize RepVGG-A0 with a standard setting of PTQ and evaluate the INT8 accuracy, which is dropped from 72.2% to 50.3%. Note that we use the deployed model after fusing multi-branches, because the unfused one would incur extra quantization errors. This trick is widely used in popular quantization frameworks.

Variants	FP32 Acc (%)	INT8 Acc (%)
RepVGG-A0 (w/ custom $L_2$ ) <sup>*</sup>	72.4	52.2 (20.2↓)
RepVGG-A0 (w/ custom $L_2$ ) <sup>†</sup>	72.2	50.3 (21.9↓)

Table 1. Quantized top-1 accuracy on ImageNet using RepVGG-A0. <sup>\*</sup>: from the official repo. <sup>†</sup>: reproduced with the official code.

We illustrate the weight distribution of our reproduced model RepVGG-A0 in Fig. 2 and Fig. 14a (appendix). Observing that the weights are well distributed around zero and no particular outlier exists, it satisfies **C1**. This leads us to verify **C2** if it is the activation that greatly deteriorates the quantization. Unfortunately, the activation is input-dependent and coupled with the learned weights through the convolutions. It’s non-trivial to theoretically draw some conclusions by hypothesizing any distribution for inputs as

well as weights. Instead, we can analyze the standard deviation of each branch relatively.

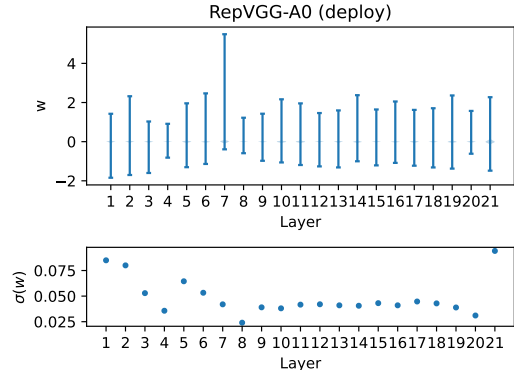


Figure 2. Violin plot and standard deviation of RepVGG-A0 convolutional weights per layer. The majority of distribution spans closely to 0 while the *min* and *max* are tractable.

Before we proceed, we formulate the computation operations in a typical RepVGG block. We keep the same naming convention as [11] to be better understood. Specifically, we use  $W_{(k)} \in \mathbb{R}^{C_2 \times C_1 \times k \times k}$  to denote the kernel of a  $k \times k$  convolution, where  $C_1$  and  $C_2$  are the number of input and output channels respectively. Note that  $k \in \{1, 3\}$  for RepVGG. As for the batch normalization (BN) layer after  $k \times k$  convolution, we use  $\mu_{(k)} \in \mathbb{R}^{C_2}$ ,  $\sigma_{(k)} \in \mathbb{R}^{C_2}$ ,  $\gamma_{(k)} \in \mathbb{R}^{C_2}$ ,  $\beta_{(k)} \in \mathbb{R}^{C_2}$  as the mean, standard deviation, scaling factor and the bias. For the BN in the identity branch, we use  $\mu_{(0)}$ ,  $\sigma_{(0)}$ ,  $\gamma_{(0)}$ ,  $\beta_{(0)}$ . Let  $M_{(1)} \in \mathbb{R}^{N \times C_1 \times H_1 \times W_1}$ ,  $M_{(2)} \in \mathbb{R}^{N \times C_2 \times H_2 \times W_2}$  be the input and output respectively, and ‘\*’ be the convolution operator. Let  $Y_{(0)}$ ,  $Y_{(1)}$  and  $Y_{(3)}$  be the output of the Identity,  $1 \times 1$  and  $3 \times 3$  branch. Without loss of generality, we suppose  $C_1 = C_2$ ,  $H_1 = H_2$ ,  $W_1 = W_2$ . Then we can write the output  $M_{(2)}$  as,

$$\begin{aligned}
 M_{(2)} &= Y_{(3)} + Y_{(1)} + Y_{(0)} \\
 &= \text{BN}(M_{(1)} * W_{(3)}, \mu_{(3)}, \sigma_{(3)}, \gamma_{(3)}, \beta_{(3)}) \\
 &\quad + \text{BN}(M_{(1)} * W_{(1)}, \mu_{(1)}, \sigma_{(1)}, \gamma_{(1)}, \beta_{(1)}) \\
 &\quad + \text{BN}(M_{(1)}, \mu_{(0)}, \sigma_{(0)}, \gamma_{(0)}, \beta_{(0)}).
 \end{aligned} \tag{2}$$

The batch normalization operation for the  $3 \times 3$  branch can be written as,

$$Y_{(3)} = \gamma_{(3)} \odot \frac{M_{(1)} * W_{(3)} - \mu_{(3)}}{\sqrt{\epsilon + \sigma_{(3)} \odot \sigma_{(3)}}} + \beta_{(3)}, \tag{3}$$

where  $\odot$  is element-wise multiplication and  $\epsilon$  a small value ( $10^{-5}$  by default) for numerical stability. This means BN plays a role of changing the statistic (mean and variance)

of its input. Note that the change of  $\mu$  doesn't necessarily affect the quantization error as it pushes the mean to zero. However, the changed variance directly affects the quantization accuracy. From the probability perspective, given a random variable  $X$ , and a scalar  $\lambda$ , the variance of  $D(\lambda X)$  equals to  $\lambda^2 D(X)$ . Let  $X_{(3)} = M^{(1)}W_{(3)}$ , then we have

$$D(Y_{(3)}) = \frac{\gamma_{(3)} \odot \gamma_{(3)}}{\epsilon + \sigma_{(3)} \odot \sigma_{(3)}} \odot D(X_{(3)}). \quad (4)$$

The value of  $\frac{\gamma_{(3)} \odot \gamma_{(3)}}{\epsilon + \sigma_{(3)} \odot \sigma_{(3)}}$  controls shrinking or expanding the variance of  $X_{(3)}$ , which in turn leads to better or worse quantization performance respectively. For  $1 \times 1$  and Identity, we can draw similar conclusions.

Based on the above analysis, we dive into the detail of RepVGG. There is a *critical but easily neglected component*, which is a special design for the weight decay called custom  $L_2$ . It is stated that this component improves the accuracy and facilitates quantization [11]. The detailed implementation is shown in Algorithm 1 (appendix).

This particular design regularizes the multi-branch weights as if it regularizes its equivalently fused kernel. It is likely to make the fused weights enjoy a quantization-friendly distribution, which can be verified by Fig. 14a (appendix). This loss `l2_loss_eq_kernel` is essentially,

$$L_{2_{custom}} = \frac{|W_{eq}|_2^2}{\left| \frac{\gamma_{(3)}}{\sqrt{\epsilon + \sigma_{(3)} \odot \sigma_{(3)}}} \right|_2^2 + \left| \frac{\gamma_{(1)}}{\sqrt{\epsilon + \sigma_{(1)} \odot \sigma_{(1)}}} \right|_2^2}. \quad (5)$$

Notably, the optimizer are encouraged to **enlarge** the denominator  $\left| \frac{\gamma_{(3)}}{\sqrt{\epsilon + \sigma_{(3)} \odot \sigma_{(3)}}} \right|_2^2 + \left| \frac{\gamma_{(1)}}{\sqrt{\epsilon + \sigma_{(1)} \odot \sigma_{(1)}}} \right|_2^2$  to minimize this loss, which **magnifies** the variance of activation and brings quantization difficulty. Apart from the theoretical analysis, we provide a simple ablation by removing the denominator from Eq 5 to have,

$$L'_{2_{custom}} = |W_{eq}|_2^2 \quad (6)$$

We report the result in Table 2. Without the denominator item, the FP32 accuracy is 71.5%, which is 0.7% lower than the baseline. However, it's surprising to see that the quantization performance is greatly **improved** to 61.2%. Although it's *still unacceptable* in practice, this experiment indicates the custom weight decay strategy  $L_2$  helps build a stronger FP32 model with decent weight distribution but it meanwhile enlarges the variance of the activation to create quantization collapse. This motivates us to drop this design and move forward.

### 3.2. Quantization-friendly Reparameterization

Here we review multiple settings (S1-S4) to resolve quantization collapse step by step.

Variants	FP32 Acc (%)	INT8 Acc (%)
RepVGG-A0 (w/ custom $L_2$ ) <sup>†</sup>	72.2	50.3 (21.9↓)
RepVGG-A0 (Eq 6)	71.5	61.2 (10.3↓)

Table 2. Removing the denominator of custom  $L_2$  improves the quantized top-1 accuracy on ImageNet. <sup>†</sup>: reproduced.

**S1 (Normal  $L_2$ ).** Based on the above discussions, we discard the custom  $L_2$  strategy and replace it with the standard weight decay. We call this setting **S1**. With this modification only, we show the result in Table 3.

While the FP32 accuracy is 0.5% lower than the baseline, its INT8 accuracy is 11.3% higher than the baseline. However, this design doesn't meet the application requirements either. Given that there are no explicit regularizers to enlarge the activation variance, it is straightforward to check the distribution of weights, which is shown in Fig. 3 and Fig. 13 (appendix). The *fused weights distribution in both Layer 5 and 6 have large standard variances* (2.4 and 5.1 respectively), which are about two orders of magnitude larger than other layers. Specifically, the maximal values of fused weights from Layer 5 and 6 are 692.1107 and 1477.3740. This explains why the quantization performance is not good. Since the quantization process of weight is independent of input or activation, violating **C1** causes unreparable error. We repeat the experiments thrice, and this phenomenon recurs.

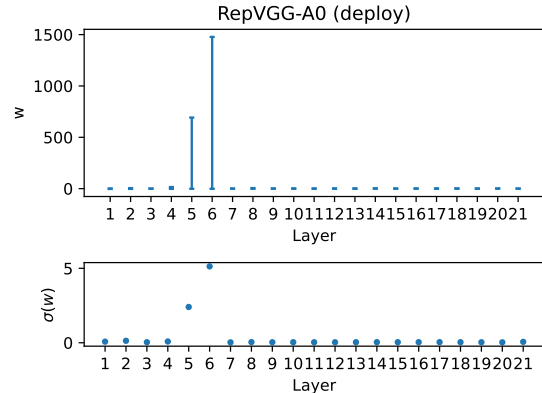


Figure 3. Violin plot of fused convolutional weights in each layer of RepVGG-A0 trained without custom  $L_2$  regularization (S1). The weight distributions of layer 5 and 6 have large variances, incurring large quantization errors (**C1 violation**).

Given that the normal  $L_2$  weight decay has been imposed for the convolution in each branch, why do some of the fused kernel weights have so big outliers? Based on Equation 2 and 3, we rewrite the equations as

Settings	Description	weight decay	C1	C2	FP32 Acc(%)	INT8 Acc(%)
<b>S0</b>	BN(3×3) + BN(1×1) + BN(Identity)	custom $L_2$	✓	✗	72.2	50.3 (21.9↓)
<b>S1</b>	BN(3×3) + BN(1×1) + BN(Identity)	normal $L_2$	✗	DC	71.7	61.6 (10.1↓)
<b>S2</b>	BN(3×3) + BN(1×1) + Identity	normal $L_2$	✓	✗	70.7	62.5 (8.2↓)
<b>S3</b>	BN(3×3) + (1×1) + Identity	normal $L_2$	✓	✓	70.1	69.5 (0.6↓)
<b>S4</b>	BN(BN(3×3) + (1×1) + Identity)	normal $L_2$	✓	✓	72.2	70.4 (1.8↓)

Table 3. Quantization-friendly design for reparameterization. **S0** is the original RepVGG, and **S4** is our proposed QARepVGG. ✓/✗ indicates whether it satisfies the condition **C1**/**C2**. DC: Don’t care as it already violates **C1**.

$$\begin{aligned}
M_{(2)} = M_{(1)} * [ & \sum_{k \in \{0,1,3\}} \text{Reshape} \left( \frac{\gamma_{(k)}}{\sqrt{\epsilon + \sigma_{(k)} \odot \sigma_{(k)}}} \right) \\
& \odot W_{(k)} ] + \sum_{k \in \{0,1,3\}} \left[ \beta_{(k)} - \frac{\gamma_{(k)} \odot \mu_{(k)}}{\sqrt{\epsilon + \sigma_{(k)} \odot \sigma_{(k)}}} \right]
\end{aligned} \tag{7}$$

where  $\text{Reshape}()$  is applied to match the computation dimension.  $W_0$  of the identity is a unit matrix, which is fixed and not decayed during the training. The learnable parameter  $(\beta, \gamma)$  of BN is routinely excluded from being decayed. Therefore, when multiplied with 1.0 from  $W_0$ , the value of  $\frac{\gamma}{\sqrt{\epsilon + \sigma^2}}$  will contribute a large value to the equivalent kernel after fusion if  $\frac{\gamma}{\sqrt{\epsilon + \sigma^2}}$  itself is large. To verify it, we illustrate the  $\frac{\gamma}{\sqrt{\epsilon + \sigma^2}}$  of three branches in Fig. 4. The maximal values of  $\frac{\gamma}{\sqrt{\epsilon + \sigma^2}}$  from the identity branch on Layer 5 and 6 are 692.1107 and 1477.3732. It’s interesting to see that the weights from the 3×3 and 1× branches from Layer 4 also have some large values but their fused weights no longer contain such values.

**S2 (Identity w/o BN).** A simple way to address the issue of **S1** to meet **C1** is to remove the BN branch from the identity branch<sup>1</sup>. We name this setting **S2** and show the result in Table 3. The error analysis on weight quantization (see Fig. 9 in the appendix) indicates this design indeed meets the requirements of **C1**. This model delivers a lower FP32 accuracy 70.7% and INT8 accuracy 62.5%, which is still infeasible. This motivates us to verify if it violates **C2**.

As the weights are obtained by minimizing the loss function across the whole training set, it’s non-trivial to reasonably derive their contributions for deviation [18]. We write the expectation of the statistics in three branches as,

$$\mathbb{E}(\mathbf{Y}_{(3)}) = \beta_{(3)}, \mathbb{E}(\mathbf{Y}_{(1)}) = \beta_{(1)}. \tag{8}$$

If  $\beta_{(3)} = \beta_{(1)} = \beta$ , these two outputs can be well aligned and their summation has a chance to enlarge the variance.

<sup>1</sup>This is equivalent to BN with fixed (non-learnable) parameters.  $\mu = 0, \sigma = 0, \gamma = 1, \beta = 0$ ,

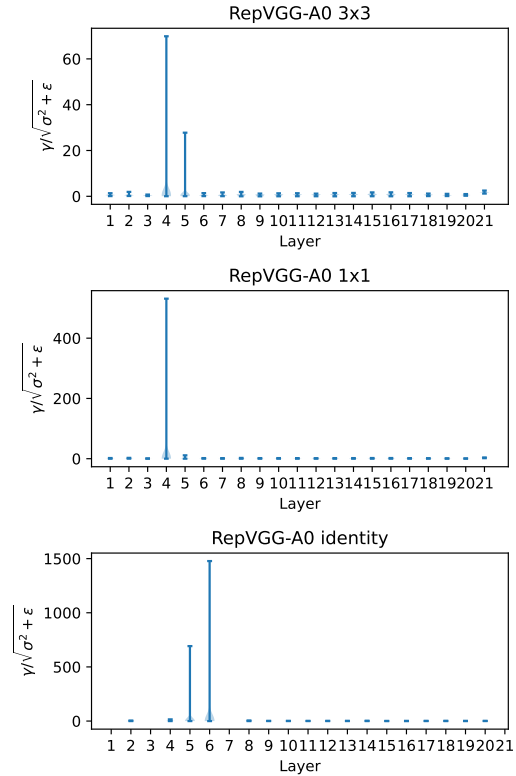


Figure 4. Violin plot of  $\gamma/\sqrt{\sigma^2 + \epsilon}$  in each layer of RepVGG-A0 trained without custom  $L_2$  regularization (**S1**). Large values influence the fused weight distribution shown in Fig. 3.

The probability of enlarging variance becomes higher if  $\beta$  is far from  $\mathbf{Y}_{(0)}$ . Next, we prove  $\beta_{(3)} = \beta_{(1)}$  as in Lemma 3.1.

**Lemma 3.1.** *Training a neural network using setting **S2** across  $n$  iterations using loss function  $l(W, \gamma, \beta)$ , for any given layer,  $\beta_{(3)}^n = \beta_{(1)}^n$ .*

*Proof.* We use mathematical induction. Without loss of generality, we use the SGD optimizer. It’s not difficult to check the validity of using other optimizers such as Adam [25].

If  $n = 0$ , then  $\beta_{(3)}^0 = \beta_{(1)}^0$  holds, since they both are initialized by  $\mathbf{0}$ .

Suppose  $n = k$ ,  $\beta_{(3)}^k = \beta_{(1)}^k$  holds.

When  $n = k + 1$ , there is no weight decay for  $\beta$ .

$$\begin{aligned} \beta_{(3)}^{k+1} &= \beta_{(3)}^k - lr^{k+1} * \frac{\partial l(W, \gamma, \beta)}{\partial \beta_{(3)}^k} \\ &= \beta_{(3)}^k - lr^{k+1} * \frac{\partial l(W, \gamma, \beta)}{\partial M_{(2)}^{k+1}} \quad (9) \\ &= \beta_{(1)}^k - lr^{k+1} * \frac{\partial l(W, \gamma, \beta)}{\partial M_{(2)}^{k+1}} = \beta_{(1)}^{k+1}. \end{aligned}$$

Q.E.D. □

ReLU [33] is the activation function in RepVGG. On one hand, it's harmful if most inputs are below zero (dead ReLU) [31]. On the other hand, it's also not favored if all inputs are above zero because of losing non-linearity. Empirically, many modern high-performance CNN models with BN often have zero means before ReLU. If we take this assumption, we would let  $E(M_{(2)}) = E(Y_{(1)} + Y_{(3)} + Y_{(0)}) = \mathbf{0}$ . Based on Lemma 3.1, we reach  $\beta_{(3)} = \beta_{(1)} = -\frac{E(Y_{(0)})}{2}$ . Note  $E(Y_{(0)}) \geq \mathbf{0}$ , adding three branches often enlarges the variance (Fig. 5).

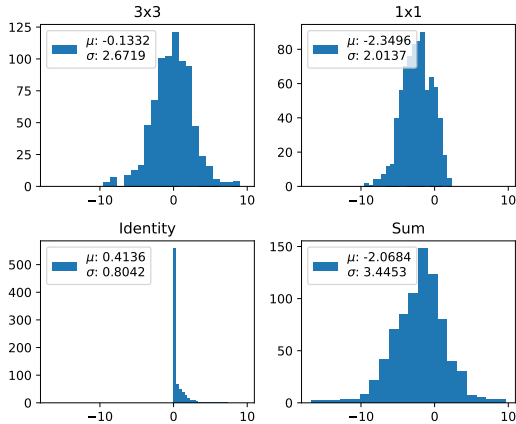


Figure 5. Enlarged variance in the activation distribution of RepVGG-A0 (S2). We pick a random image from the ImageNet validation set and draw the output (channel 0) of each branch at layer 4 (it is also easily seen in other layers and channels).

**S3 (No BN for Identity and 1×1).** If  $3 \times 3$  and  $1 \times 1$  have the same mean, their summation is prone to enlarging the variance. To better control the variance, we further remove the BN in  $1 \times 1$  branch. We name this setting S3 and show the result in Table 3. This design achieves 70.1% top-1 FP32 accuracy and 69.5% INT 8 accuracy on ImageNet, which greatly improves the quantization performance. However, the FP32 accuracy is still low.

**S4 (Post BN on S3)** Since the addition of the three branches introduces the covariate shift issue [23], we append an extra batch normalization after the addition of three branches to stabilize the training process and name this setting S4 (Fig. 1 right). The post BN doesn't affect the equivalent kernel fusion for deployment. This further boosts the FP32 accuracy of our A0 model from 70.1% to 72.2% on ImageNet. Moreover, its INT8 accuracy is enhanced to 70.4%. So far, we have substantially resolved the quantization failure and refer the network under S4 as QARepVGG.

## 4. Experiment

### 4.1. Settings

We mainly focus our experiments on ImageNet dataset [5]. And we verify the generalization of our method based on a recent popular detector YOLOv6 [28], which extensively adopts the reparameterization design. As for PTQ, we use the Pytorch-Quantization toolkit [34], which is widely used in deployment on NVIDIA GPUs. Weights, inputs to convolution layers and full connection layers are all quantized into 8-bit, including the first and last layer. Following the default setting of Pytorch-Quantization toolkit, the quantization scheme is set to *symmetric uniform*. We use the same settings and the calibration dataset for all the quantization results, except those officially reported ones.

### 4.2. ImageNet Classification

To make fair comparisons, we strictly control the training settings as [11]. As for model specification, we use the same configuration as [11] except for the quantization-friendly reparameterization design, which includes the A and B series. This naturally generates the same deploy model for inference. All models are trained for 120 epochs with a global batch size of 256. We use SGD optimizer with a momentum of 0.9 and a weight decay of  $10^{-4}$ . The learning rate is initialized as 0.1 and decayed to zero following a cosine strategy. We also follow the simple data augmentations as [11]. All experiments are done on 8 Tesla-V100 GPUs.

The results are shown in Table 4. Our models achieve comparable FP32 accuracy as RepVGG. Notably, RepVGG severely suffers from quantization, where its INT8 accuracy largely lags behind its FP32 counterpart. For example, the top-1 accuracy of RepVGG-B0 is dropped to 40.2% from 75.1%. In contrast, our method exhibits strong INT8 performance, where the accuracy drops are within 2%.

We observe that RepVGG with group convolutions behaves much worse. The accuracy of RepVGG-B2g4 is dropped from 78.5% to 13.7% after PTQ (64.8%↓). Whereas, our QARepVGG-B2g4 only loses 0.7% accuracy, indicating its robustness to other scales and variants.

Model	FP32 (%)	INT8 (%)	FPS	Params M	FLOPs B
RepVGG-A0 <sup>‡</sup>	72.4	52.2	3256	8.30	1.4
RepVGG-A0 <sup>†</sup>	72.2	50.3	3256	8.30	1.4
QARepVGG-A0	72.2	<b>70.4</b>	3256	8.30	1.4
RepVGG-B0 <sup>‡</sup>	75.1	40.2	1817	14.33	3.1
QARepVGG-B0	74.8	<b>72.9</b>	1817	14.33	3.1
RepVGG-B1g4 <sup>‡</sup>	77.6	0.55	868	36.12	7.3
QARepVGG-B1g4	77.4	<b>76.5</b>	868	36.12	7.3
RepVGG-B1g2 <sup>‡</sup>	77.8	14.5	792	41.36	8.8
QARepVGG-B1g2	77.7	<b>77.0</b>	792	41.36	8.8
RepVGG-B1 <sup>†</sup>	78.4	3.4	685	51.82	11.8
QARepVGG-B1	78.0	<b>76.4</b>	685	51.82	11.8
RepVGG-B2g4 <sup>‡</sup>	78.5	13.7	581	55.77	11.3
QARepVGG-B2g4	78.4	<b>77.7</b>	581	55.77	11.3
RepVGG-B2 <sup>‡</sup>	78.8	51.3	460	80.31	18.4
QARepVGG-B2	79.0	<b>77.7</b>	460	80.31	18.4

Table 4. Classification results on ImageNet validation dataset. All models are trained under the same settings and are evaluated in deploy mode. <sup>†</sup>: reproduced. <sup>‡</sup>: RepVGG official.

### 4.3. Ablation Study

**Variants Architecture Design.** We study the quantization performance on variant designs and show the results in Table 5. Note that when BN is entirely removed, the model fails to converge. Though the setting with post BN only has 71.1% INT8 top-1 accuracy, its FP32 accuracy is low. The quantization gap is enlarged as the model capacity grows (from A0 to B0), which disapproves of this approach.

Model Variants	$L_{2_{custom}}$	FP32 (%)	INT8 (%)
RepVGG-A0*	✓	72.4	52.2
All w/ BN, w/ Post BN	✓	72.2	58.7
QARepVGG-A0 (S4)	✗	72.2	70.4
QARepVGG-A0 w/o Post BN (S3)	✗	70.1	69.5
All w/o BN, w/ Post BN	✗	71.7	71.1
All w/o BN, w/o Post BN	✗	0.1	0.1
All w/ BN excl. ID, w/ Post BN	✗	71.6	62.9
All w/ BN excl. ID, w/o Post BN (S2)	✗	70.7	62.5
RepVGG-B0	✓	75.1	40.2
QARepVGG-B0	✗	74.8	72.9
All w/o BN, w/ Post BN	✗	73.7	73.1

Table 5. Ablation study on architectural designs evaluated on ImageNet. \*: from the official repo. All: All branches, w/: with, w/o: without, excl. : excluding.

Model	FP32 acc (%)	INT8 acc (%)	Epochs
RepOpt-VGG-A0	70.3	64.8 (5.5↓)	240 <sup>‡</sup> +120
QARepVGG-A0	72.2	70.4 (1.8↓)	120
RepOpt-VGG-B0	73.8	62.6 (11.2↓)	240 <sup>‡</sup> +120
QARepVGG-B0	74.8	72.9 (1.9↓)	120
RepOpt-VGG-B1*	78.5	75.9 (2.6↓)	240 <sup>‡</sup> +120
RepOpt-VGG-B1 <sup>†</sup>	78.3	75.9 (2.4↓)	240 <sup>‡</sup> +120
QARepVGG-B1	78.0	76.4 (1.6 ↓)	120

Table 6. Comparison with RepOpt-VGG on ImageNet dataset. \*: official repo. <sup>†</sup>: reproduced. <sup>‡</sup>: 240 epochs on CIFAR-100

**Comparison with RepOpt-VGG [7].** RepOpt-VGG [7] uses gradient reparameterization and it contains two stages: searching the scales and training with the scales obtained. Quantization accuracy can be very sensitive depending on the search quality of scales [7].

As only a few pre-trained models are released, we retrain RepOpt-VGG-A0/B0 models following [7]. Namely, we run a hyper-parameter searching for 240 epochs on CIFAR-100 [27] and train for a complete 120 epochs on ImageNet. We can reproduce the result of RepOpt-VGG-B1 with the officially released scales. However, it was hard to find out good scales for A0/B0 to have comparable performance. As shown in Table 6, RepOpt-VGG-A0 achieves 70.3% on ImageNet, which is 2.1% lower than RepVGG. Although being much better than RepVGG, their PTQ accuracies are still too low<sup>2</sup>. In contrast, our method outperforms RepOpt with clear margins. Besides, we don’t have sensitive hyper-parameters or extra training costs.

**Error Analysis.** To understand how the quantization error propagates, we perform per-layer MSE analysis of RepVGG-A0 and QARepVGG-A0 in Fig. 6. RepVGG-A0 is more sensitive to quantization and runs into collapse as the cumulative errors become intolerable. Given that RepVGG-A0 satisfies C1, we sample a batch of images to depict the difference between the two regarding C2 in Fig. 7. Our method produces a better activation distribution of smaller standard variances and min/max values, hence ensuring better quantization performance.

**QAT for QARepVGG.** Quantization-aware training is typically used to further improve performance. However, it is not straightforward to apply QAT to RepVGG [7]. In contrast, it’s simple to apply it on QARepVGG where its post BN can be reserved to facilitate the training. All models shown in Table 7 are trained for 10 epochs (the first three ones for warm-up) with an initial learning rate of 0.01. The

<sup>2</sup>See error analysis for RepOpt-VGG-B0 in Fig. 10 (appendix).

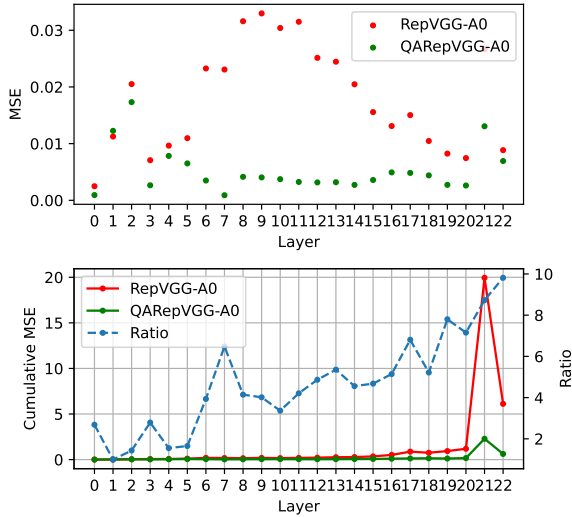


Figure 6. **Top:** Sensitivity analysis (switching on only one layer in INT8 and comparing it with its FP32 counterpart) of QARepVGG-A0 vs. RepVGG-A0. **Bottom:** Cumulative MSE is tested by sequentially switching on layers one after another in INT8. The blue-dashed line indicates the relative ratio between the two.

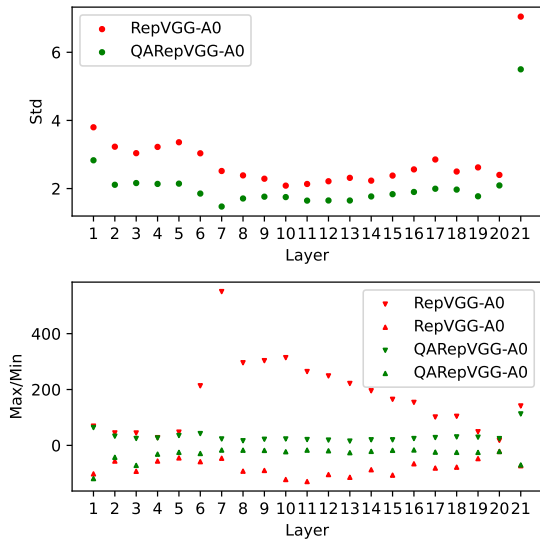


Figure 7. Standard variance and max/min value of feature maps (the same batch is used) before activation of each QARepVGG-A0 block compared with RepVGG-A0.

quantization gap for QARepVGG is enclosed within 0.3%.

#### 4.4. Object Detection

To further verify the generalization of QARepVGG, we test it on object detectors like YOLOv6 [28]. It extensively makes use of RepVGG blocks and severely suffers from the quantization issue. Although YOLOv6 alleviates this issue

Model	FP32 acc (%)	PTQ acc (%)	QAT acc (%)
QARepVGG-A0	72.2	70.4 (1.8↓)	71.9 (0.3↓)
QARepVGG-B0	74.8	72.9 (1.9↓)	74.6 (0.2↓)

Table 7. QAT results for QARepVGG on ImageNet validation set.

Model	FP32 mAP (%)	INT8 mAP (%)	Epochs
YOLOv6t-RepVGG	40.8	37.8 (3.0↓)	300
YOLOv6t-RepOpt	40.7	39.1 (1.6↓)	300+300
YOLOv6t-QARepVGG	40.7	39.5 (1.2↓)	300
YOLOv6s-RepVGG*	42.4	35.0 (7.4↓)	300
YOLOv6s-RepOpt*	42.4	40.9 (1.5↓)	300+300
YOLOv6s-QARepVGG	42.3	41.0 (1.3↓)	300

Table 8. Detection results on COCO. \*: from the official repo.

by resorting to RepOpt-VGG [7], the approach is unstable and requires careful hyperparameter tuning.

We take ‘tiny’ and ‘small’ model variants as comparison benchmarks. We train and evaluate QARepVGG-fashioned YOLOv6 on the COCO 2017 dataset [29] and exactly follow its official settings [28]. The results are shown in Table 8. RepVGG and QARepVGG versions are trained for 300 epochs on 8 Tesla-V100 GPUs. RepOpt requires extra 300 epochs to search for scales.

Noticeably, YOLOv6s-RepVGG suffers a huge quantization degradation for about 7.4% mAP via PTQ. YOLOv6t-RepVGG is slightly better, but the reduction of 3% mAP is again unacceptable in practical deployment. Contrarily, YOLOv6s/t-QARepVGG have similar FP32 accuracies to their RepVGG counterpart, while INT8 accuracy drops are restricted within 1.3% mAP. YOLOv6-RepOpt-VGG could give better PTQ accuracy than YOLOv6-RepVGG as well. However, it requires a doubled cost. We also find that the final accuracy of RepOpt-VGG is quite sensitive to the searched hyperparameters which cannot be robustly obtained.

## 5. Conclusion

Through theoretical and quantitative analysis, we dissect the well-known quantization failure of the notable reparameterization-based structure RepVGG. Its structural defect inevitably magnifies the quantization error and cumulatively produces inferior results. We refashion its design to have QARepVGG, which generates the weight and activation distributions that are advantageous for quantization. QARepVGG greatly eases the quantization process for final deployment. We emphasize that quantization awareness in architectural design shall be drawn more attention.



## References

- [1] Haoping Bai, Meng Cao, Ping Huang, and Jiulong Shan. Batchquant: Quantized-for-all architecture search with robust quantizer. *Advances in Neural Information Processing Systems*, 34:1074–1085, 2021. [2](#)
- [2] Yash Bhalgat, Jinwon Lee, Markus Nagel, Tijmen Blankevoort, and Nojun Kwak. Lsq+: Improving low-bit quantization through learnable offsets and better initialization. In *Proceedings of the IEEE/CVF Conference on Computer Vision and Pattern Recognition Workshops*, pages 696–697, 2020. [1](#), [2](#)
- [3] Yaohui Cai, Zhewei Yao, Zhen Dong, Amir Gholami, Michael W Mahoney, and Kurt Keutzer. Zeroq: A novel zero shot quantization framework. In *Proceedings of the IEEE/CVF Conference on Computer Vision and Pattern Recognition*, pages 13169–13178, 2020. [2](#)
- [4] Liang-Chieh Chen, George Papandreou, Iasonas Kokkinos, Kevin Murphy, and Alan L Yuille. Deeplab: Semantic image segmentation with deep convolutional nets, atrous convolution, and fully connected crfs. *IEEE transactions on pattern analysis and machine intelligence*, 40(4):834–848, 2017. [1](#)
- [5] Jia Deng, Wei Dong, Richard Socher, Li-Jia Li, Kai Li, and Li Fei-Fei. Imagenet: A large-scale hierarchical image database. In *2009 IEEE conference on computer vision and pattern recognition*, pages 248–255. Ieee, 2009. [6](#)
- [6] Jacob Devlin, Ming-Wei Chang, Kenton Lee, and Kristina Toutanova. Bert: Pre-training of deep bidirectional transformers for language understanding. In *Proceedings of the 2019 Conference of the North American Chapter of the Association for Computational Linguistics: Human Language Technologies, Volume 1 (Long and Short Papers)*, pages 4171–4186, 2019. [1](#)
- [7] Xiaohan Ding, Honghao Chen, Xiangyu Zhang, Kaiqi Huang, Jungong Han, and Guiguang Ding. Re-parameterizing your optimizers rather than architectures. *arXiv preprint arXiv:2205.15242*, 2022. [1](#), [2](#), [3](#), [7](#), [8](#)
- [8] Xiaohan Ding, Yuchen Guo, Guiguang Ding, and Jungong Han. Acnet: Strengthening the kernel skeletons for powerful cnn via asymmetric convolution blocks. In *Proceedings of the IEEE/CVF international conference on computer vision*, pages 1911–1920, 2019. [1](#)
- [9] Xiaohan Ding, Xiangyu Zhang, Jungong Han, and Guiguang Ding. Diverse branch block: Building a convolution as an inception-like unit. In *Proceedings of the IEEE/CVF Conference on Computer Vision and Pattern Recognition*, pages 10886–10895, 2021. [2](#)
- [10] Xiaohan Ding, Xiangyu Zhang, Jungong Han, and Guiguang Ding. Scaling up your kernels to 31x31: Revisiting large kernel design in cnns. In *Proceedings of the IEEE/CVF Conference on Computer Vision and Pattern Recognition*, pages 11963–11975, 2022. [1](#)
- [11] Xiaohan Ding, Xiangyu Zhang, Ningning Ma, Jungong Han, Guiguang Ding, and Jian Sun. Repvgg: Making vgg-style convnets great again. In *Proceedings of the IEEE/CVF Conference on Computer Vision and Pattern Recognition*, pages 13733–13742, 2021. <https://github.com/DingXiaoH/RepVGG.git>, hashtag: 5c2e359a144726b9d14cba1e455bf540eaa54afc. [1](#), [2](#), [3](#), [4](#), [6](#), [10](#)
- [12] Alexey Dosovitskiy, Lucas Beyer, Alexander Kolesnikov, Dirk Weissenborn, Xiaohua Zhai, Thomas Unterthiner, Mostafa Dehghani, Matthias Minderer, Georg Heigold, Sylvain Gelly, et al. An image is worth 16x16 words: Transformers for image recognition at scale. In *International Conference on Learning Representations*, 2020. [1](#)
- [13] Alex Graves, Abdel-rahman Mohamed, and Geoffrey Hinton. Speech recognition with deep recurrent neural networks. In *2013 IEEE international conference on acoustics, speech and signal processing*, pages 6645–6649. Ieee, 2013. [1](#)
- [14] Suyog Gupta, Ankur Agrawal, Kailash Gopalakrishnan, and Pritish Narayanan. Deep learning with limited numerical precision. In *International conference on machine learning*, pages 1737–1746. PMLR, 2015. [1](#)
- [15] Philipp Gysel, Jon Pimentel, Mohammad Motamedi, and Soheil Ghiasi. Ristretto: A framework for empirical study of resource-efficient inference in convolutional neural networks. *IEEE transactions on neural networks and learning systems*, 29(11):5784–5789, 2018. [1](#)
- [16] Hai Victor Habi, Reuven Peretz, Elad Cohen, Lior Dikstein, Oranit Dror, Idit Diamant, Roy H Jennings, and Arnon Netzer. Hptq: Hardware-friendly post training quantization. *arXiv preprint arXiv:2109.09113*, 2021. [1](#), [2](#)
- [17] Kaiming He, Georgia Gkioxari, Piotr Dollár, and Ross Girshick. Mask r-cnn. In *Proceedings of the IEEE international conference on computer vision*, pages 2961–2969, 2017. [1](#)
- [18] Kaiming He, Xiangyu Zhang, Shaoqing Ren, and Jian Sun. Delving deep into rectifiers: Surpassing human-level performance on imagenet classification. In *Proceedings of the IEEE international conference on computer vision*, pages 1026–1034, 2015. [5](#)
- [19] Kaiming He, Xiangyu Zhang, Shaoqing Ren, and Jian Sun. Deep residual learning for image recognition. In *Proceedings of the IEEE conference on computer vision and pattern recognition*, pages 770–778, 2016. [1](#)
- [20] Andrew Howard, Mark Sandler, Grace Chu, Liang-Chieh Chen, Bo Chen, Mingxing Tan, Weijun Wang, Yukun Zhu, Ruoming Pang, Vijay Vasudevan, et al. Searching for mobilenetv3. In *Proceedings of the IEEE/CVF international conference on computer vision*, pages 1314–1324, 2019. [1](#)
- [21] Andrew G Howard, Menglong Zhu, Bo Chen, Dmitry Kalenichenko, Weijun Wang, Tobias Weyand, Marco Andreetto, and Hartwig Adam. Mobilenets: Efficient convolutional neural networks for mobile vision applications. *arXiv preprint arXiv:1704.04861*, 2017. [1](#)
- [22] Mu Hu, Junyi Feng, Jiashen Hua, Baisheng Lai, Jianqiang Huang, Xiaojin Gong, and Xian-Sheng Hua. Online convolutional re-parameterization. In *Proceedings of the IEEE/CVF Conference on Computer Vision and Pattern Recognition*, pages 568–577, 2022. [1](#), [10](#)
- [23] Sergey Ioffe and Christian Szegedy. Batch normalization: Accelerating deep network training by reducing internal covariate shift. In *International conference on machine learning*, pages 448–456. PMLR, 2015. [6](#)
- [24] Benoit Jacob, Skirmantas Kligys, Bo Chen, Menglong Zhu, Matthew Tang, Andrew Howard, Hartwig Adam, and Dmitry

- Kalenichenko. Quantization and training of neural networks for efficient integer-arithmetic-only inference. In *Proceedings of the IEEE conference on computer vision and pattern recognition*, pages 2704–2713, 2018. 2
- [25] Diederik P Kingma and Jimmy Ba. Adam: A method for stochastic optimization. In *ICLR*, 2014. 5
- [26] Raghuraman Krishnamoorthi. Quantizing deep convolutional networks for efficient inference: A whitepaper. *arXiv preprint arXiv:1806.08342*, 2018. 1
- [27] Alex Krizhevsky, Geoffrey Hinton, et al. Learning multiple layers of features from tiny images. 2009. 7
- [28] Chuyi Li, Lulu Li, Hongliang Jiang, Kaiheng Weng, Yifei Geng, Liang Li, Zaidan Ke, Qingyuan Li, Meng Cheng, Weiqiang Nie, Yiduo Li, Bo Zhang, Yufei Liang, Linyuan Zhou, Xiaoming Xu, Xiangxiang Chu, Xiaoming Wei, and Xiaolin Wei. Yolov6: a single-stage object detection framework for industrial applications. *arXiv preprint arXiv:2209.02976*, 2022. <https://github.com/meituan/YOLOv6.git>, hashtag: 05da1477671017ac2edbb709e09c75854a7b4eb1. 1, 2, 6, 8
- [29] Tsung-Yi Lin, Michael Maire, Serge Belongie, James Hays, Pietro Perona, Deva Ramanan, Piotr Dollár, and C Lawrence Zitnick. Microsoft coco: Common objects in context. In *European conference on computer vision*, pages 740–755. Springer, 2014. 8
- [30] Renjie Liu. Higher accuracy on vision models with EfficientNet-Lite. <https://blog.tensorflow.org/2020/03/higher-accuracy-on-vision-models-with-efficientnet-lite.html>, 2020. 2
- [31] Andrew L Maas, Awni Y Hannun, Andrew Y Ng, et al. Rectifier nonlinearities improve neural network acoustic models. In *ICML*, volume 30, page 3. Atlanta, Georgia, USA, 2013. 6
- [32] Markus Nagel, Mart van Baalen, Tijmen Blankevoort, and Max Welling. Data-free quantization through weight equalization and bias correction. In *Proceedings of the IEEE/CVF International Conference on Computer Vision*, pages 1325–1334, 2019. 2
- [33] Vinod Nair and Geoffrey E Hinton. Rectified linear units improve restricted boltzmann machines. In *ICML*, 2010. 6
- [34] NVIDIA. TensorRT. <https://developer.nvidia.com/tensorrt>, 2018. 6
- [35] Joseph Redmon, Santosh Divvala, Ross Girshick, and Ali Farhadi. You only look once: Unified, real-time object detection. In *Proceedings of the IEEE conference on computer vision and pattern recognition*, pages 779–788, 2016. 1
- [36] Mark Sandler, Andrew Howard, Menglong Zhu, Andrey Zhmoginov, and Liang-Chieh Chen. Mobilenetv2: Inverted residuals and linear bottlenecks. In *Proceedings of the IEEE conference on computer vision and pattern recognition*, pages 4510–4520, 2018. 1
- [37] Tao Sheng, Chen Feng, Shaojie Zhuo, Xiaopeng Zhang, Liang Shen, and Mickey Aleksic. A quantization-friendly separable convolution for mobilenets. In *2018 1st Workshop on Energy Efficient Machine Learning and Cognitive Computing for Embedded Applications (EMC2)*, pages 14–18. IEEE, 2018. 1, 2
- [38] Mingxing Tan and Quoc Le. Efficientnet: Rethinking model scaling for convolutional neural networks. In *International Conference on Machine Learning*, pages 6105–6114. PMLR, 2019. 1
- [39] Pavan Kumar Anasosalu Vasu, James Gabriel, Jeff Zhu, Oncel Tuzel, and Anurag Ranjan. An improved one millisecond mobile backbone. *arXiv preprint arXiv:2206.04040*, 2022. 1, 2
- [40] Ashish Vaswani, Noam Shazeer, Niki Parmar, Jakob Uszkoreit, Llion Jones, Aidan N Gomez, Łukasz Kaiser, and Illia Polosukhin. Attention is all you need. *Advances in neural information processing systems*, 30, 2017. 1
- [41] Chien-Yao Wang, Alexey Bochkovskiy, and Hong-Yuan Mark Liao. Yolov7: Trainable bag-of-freebies sets new state-of-the-art for real-time object detectors. *arXiv preprint arXiv:2207.02696*, 2022. 1, 2
- [42] Kuan Wang, Zhijian Liu, Yujun Lin, Ji Lin, and Song Han. Haq: Hardware-aware automated quantization with mixed precision. In *Proceedings of the IEEE/CVF Conference on Computer Vision and Pattern Recognition*, pages 8612–8620, 2019. 2
- [43] Bichen Wu, Yanghan Wang, Peizhao Zhang, Yuandong Tian, Peter Vajda, and Kurt Keutzer. Mixed precision quantization of convnets via differentiable neural architecture search. *arXiv preprint arXiv:1812.00090*, 2018. 2
- [44] Shangliang Xu, Xinxin Wang, Wenyu Lv, Qinyao Chang, Cheng Cui, Kaipeng Deng, Guanzhong Wang, Qingqing Dang, Shengyu Wei, Yuning Du, et al. Pp-yoloe: An evolved version of yolo. *arXiv preprint arXiv:2203.16250*, 2022. 1, 2
- [45] Stone Yun and Alexander Wong. Do all mobilenets quantize poorly? gaining insights into the effect of quantization on depthwise separable convolutional networks through the eyes of multi-scale distributional dynamics. In *Proceedings of the IEEE/CVF Conference on Computer Vision and Pattern Recognition*, pages 2447–2456, 2021. 1
- [46] Sergey Zagoruyko and Nikos Komodakis. Diracnets: Training very deep neural networks without skip-connections. *arXiv preprint arXiv:1706.00388*, 2017. 1

## A. Algorithm

We give the custom  $L_2$  implementation in Alg. 1.

## B. Comparison

OREPA [22] proposes a two-stage pipeline to reduce the huge training overhead of RepVGG [11]. To achieve this goal, they introduce linear scaling layers to replace to the training-time non-linear norm layers, which could maintain optimization diversity and the enhancement of the representational capacity. We evaluate the the official released pre-trained models to obtain its PTQ performance, including OREPA-RepVGG-A0, A1 and A2. As shown in Table 9, OREPA could achieve an enjoyable FP32 accuracy, while its PTQ results is far from satisfaction. Particularly,

**Algorithm 1** The code of custom  $L_2$  in RepVGG block.

```
def get_custom_L2(self):
    K3 = self.rbr_dense.conv.weight # 3x3
    K1 = self.rbr_1x1.conv.weight # 1x1
    t3 = (self.rbr_dense.bn.weight / ((self.rbr_dense.bn.running_var + self.rbr_dense.bn.eps).sqrt())).reshape(-1, 1, 1, 1).detach()
    t1 = (self.rbr_1x1.bn.weight / ((self.rbr_1x1.bn.running_var + self.rbr_1x1.bn.eps).sqrt())).reshape(-1, 1, 1, 1).detach()
    l2_loss_circle = (K3 ** 2).sum() - (K3[:, :, 1:2, 1:2] ** 2).sum()
    eq_kernel = K3[:, :, 1:2, 1:2] * t3 + K1 * t1
    l2_loss_eq_kernel = (eq_kernel ** 2 / (t3 ** 2 + t1 ** 2)).sum() # Normalize
    return l2_loss_eq_kernel + l2_loss_circle
```

OREPA-RepVGG-A2 suffers an accuracy drop of 13.5% via PTQ.

Variants	FP32 Acc (%)	INT8 Acc (%)
OREPA-RepVGG-A0	73.04	63.24 (9.80↓)
OREPA-RepVGG-A1	74.85	66.35 (8.50↓)
OREPA-RepVGG-A2	76.72	63.21 (13.51↓)

Table 9. PTQ performance for OREPA on ImageNet.

**C. Figures**

**C.1. Summary of Experiments**

For a handy reference, we give the complete list of experiments and corresponding figures and tables in Table. 10.

Method	Tables	Weight	Activation	MSE
S0	Table 1, 2, 3	Fig. 2, (14a app.)	Fig. 7	Fig. 6
Eq 6	Table 2	Fig. (8, 14b, 16 app.)		
S1	Table 3	Fig. 3, 4, (13, 15 app.)		
S2	Table 3, 5	Fig. 12, (12 app.)	Fig. 5	Fig. (9 app.)
S3	Table 3, 5			
S4	Table 3, 5	Fig. (17 app.)	Fig. 7	Fig. 6
RepVGG-B1	Table 4			Fig. (11 app.)
RepVGG-B1g4	Table 4			Fig. (11 app.)
RepOpt-VGG-B0	Table 6			Fig. (10 app.)
QARepVGG (QAT)	Table 7			
YOLOv6-QARepVGG	Table 8			

Table 10. Complete list of experiments and corresponding figures and tables. app. : appendix

**C.2. Weight Distribution**

Due to built-in weight normalization, either custom L2 or vanilla L2, the convolutional weights generally center around 0 and span unbiasedly for RepVGG-A0, see Figure 14. We also show the violin plot of RepVGG-A0

trained removing the coefficient  $\gamma/\sqrt{\sigma^2 + \epsilon}$  in  $L_2$  in Figure 8. These figures show one of the priors is satisfied to be quantization-friendly.

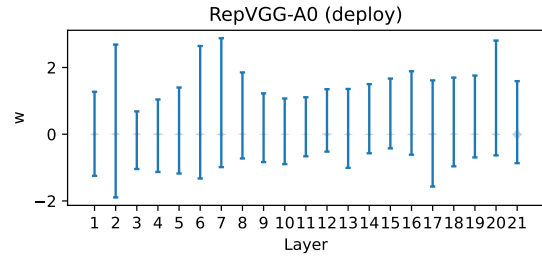


Figure 8. Violin plot of RepVGG-A0 convolutional weights when trained removing  $\gamma/\sqrt{\sigma^2 + \epsilon}$  in  $L_2$ .

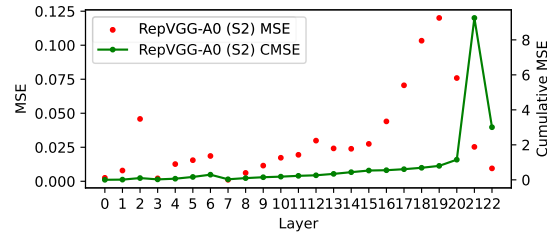


Figure 9. MSE and Cumulative MSE of RepVGG-A0 (S2).

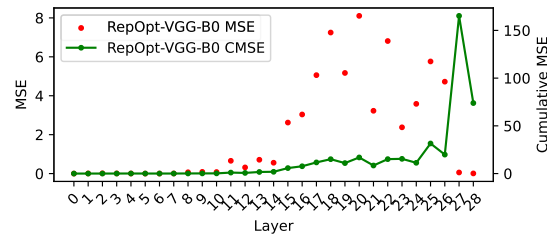
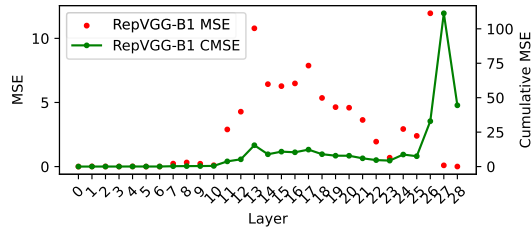
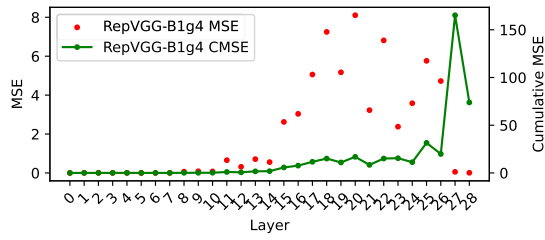


Figure 10. MSE and Cumulative MSE of RepOpt-VGG-B0.



(a) RepVGG-B1



(b) RepVGG-B1g4

Figure 11. MSE and Cumulative MSE of RepVGG-B1 and RepVGG-B1g4.

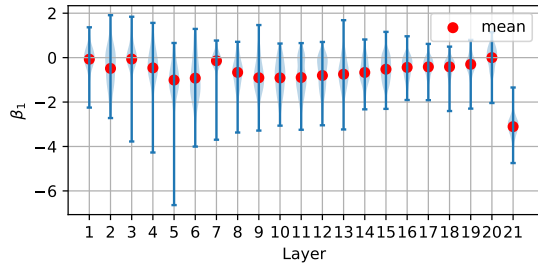
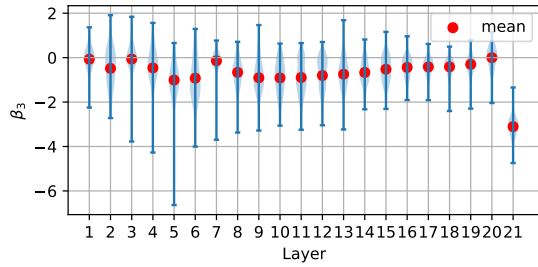


Figure 12. BN bias distribution of RepVGG-A0 convolutional weights trained in S2.  $\beta_i$  for BN after Conv  $i \times i$ .

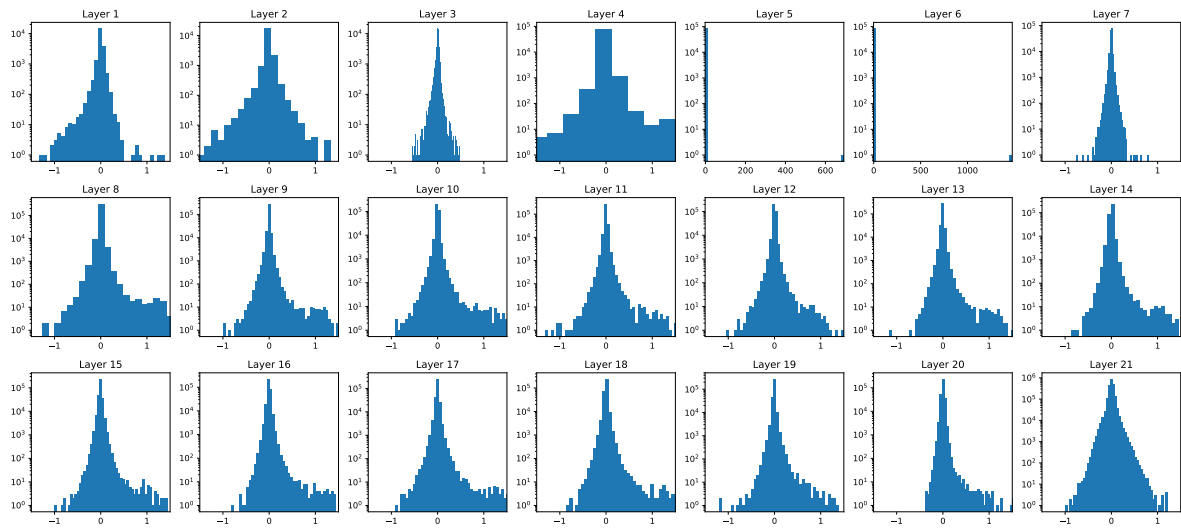
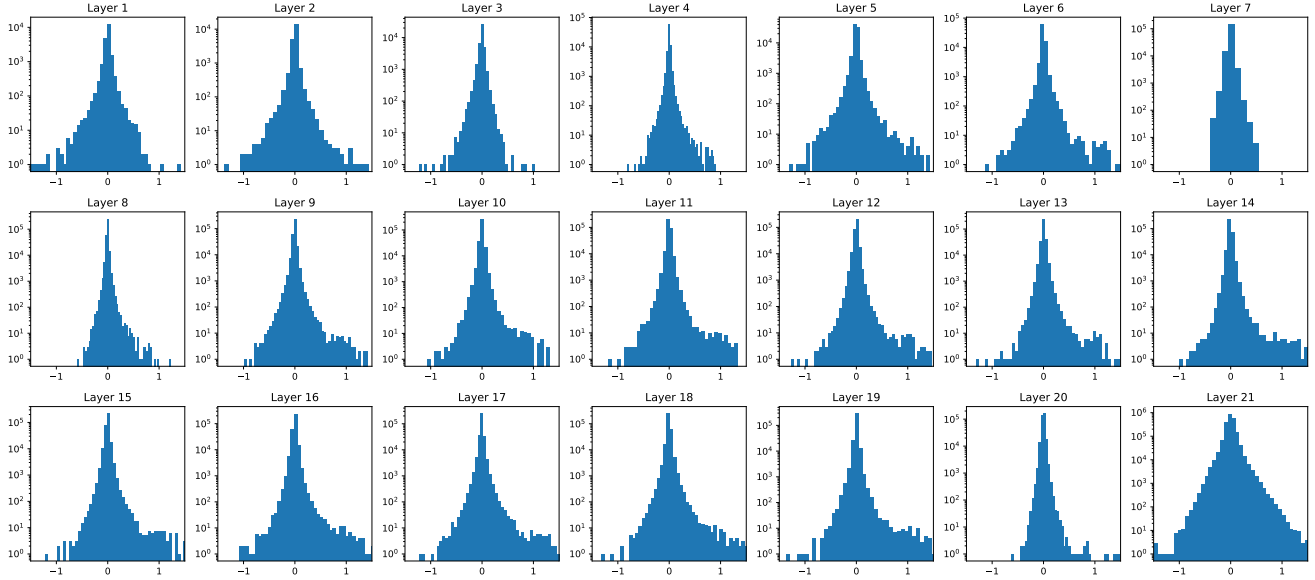
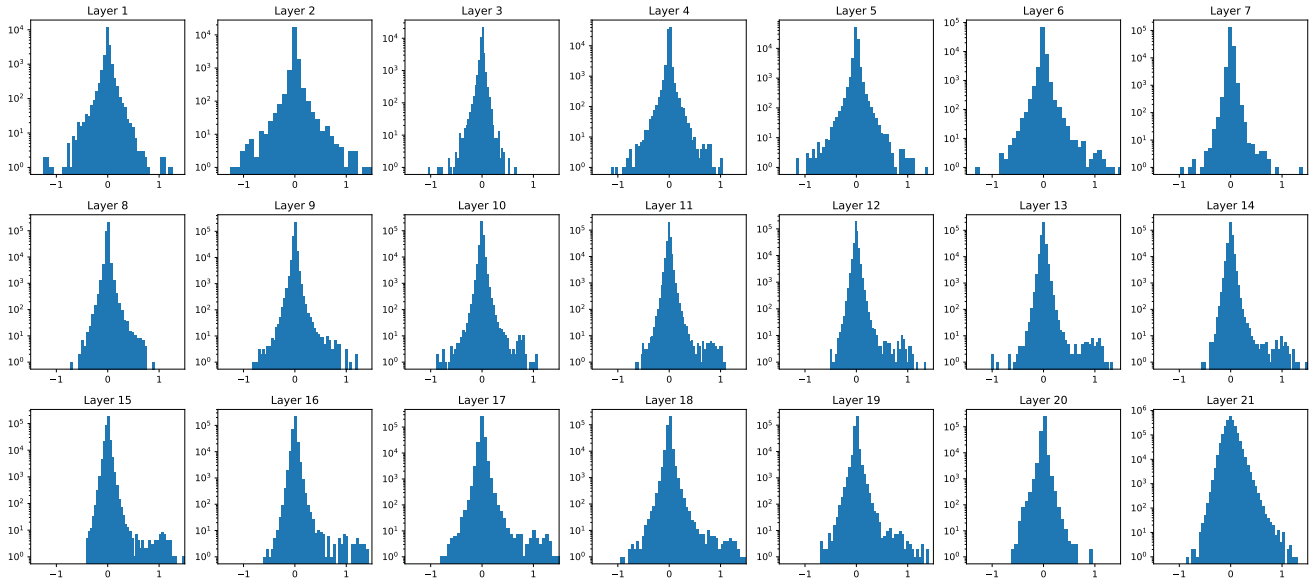


Figure 13. Distribution of RepVGG-A0 fused convolutional weights trained without custom  $L_2$  regularization (S1). Layer 5 and 6 becomes intractable and violate C1.

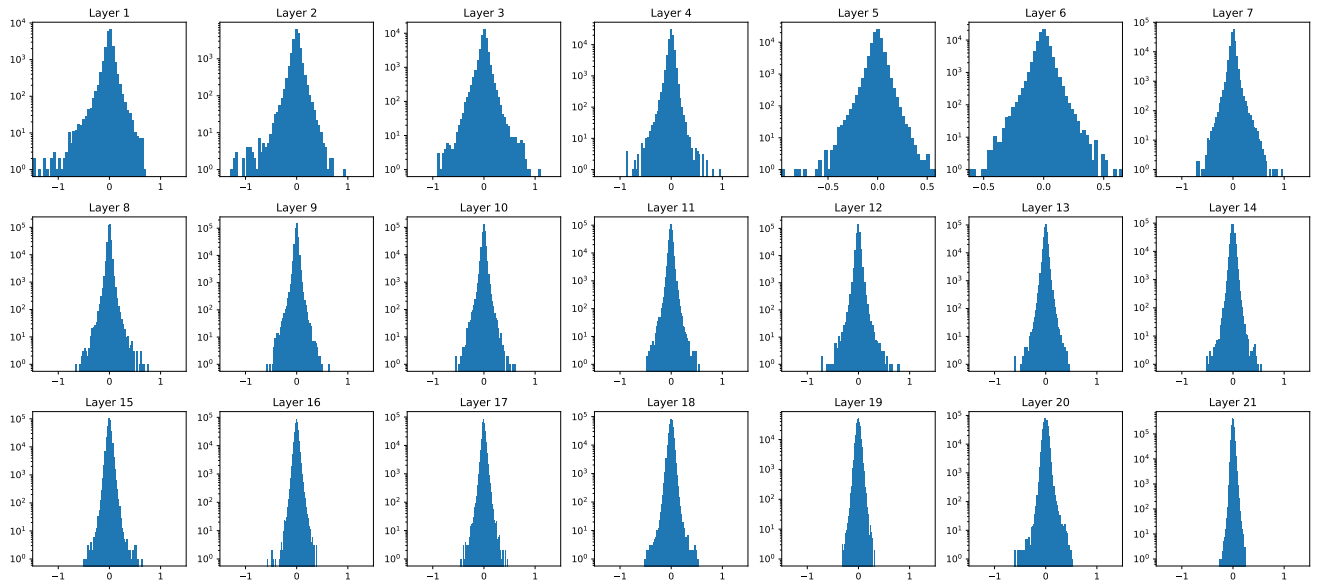


(a) RepVGG-A0 trained with the default custom  $L_2$

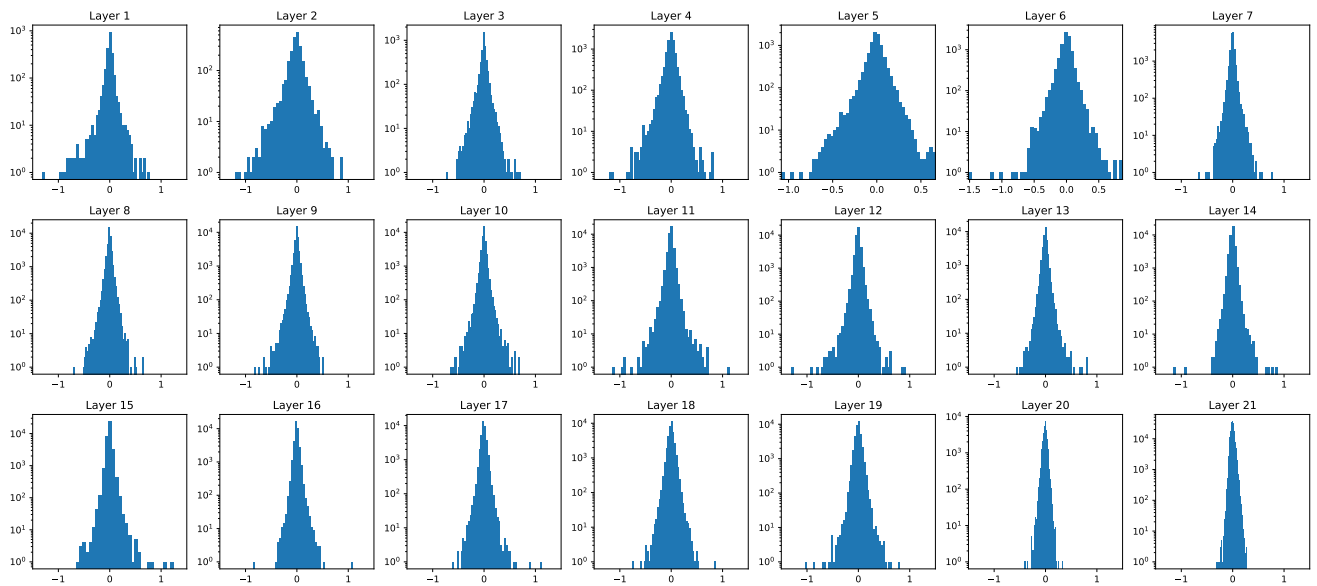


(b) RepVGG-A0 trained removing  $\gamma/\sqrt{\sigma^2 + \epsilon}$  in custom  $L_2$

Figure 14. Fused weight distribution of RepVGG-A0 trained under different  $L_2$  settings.

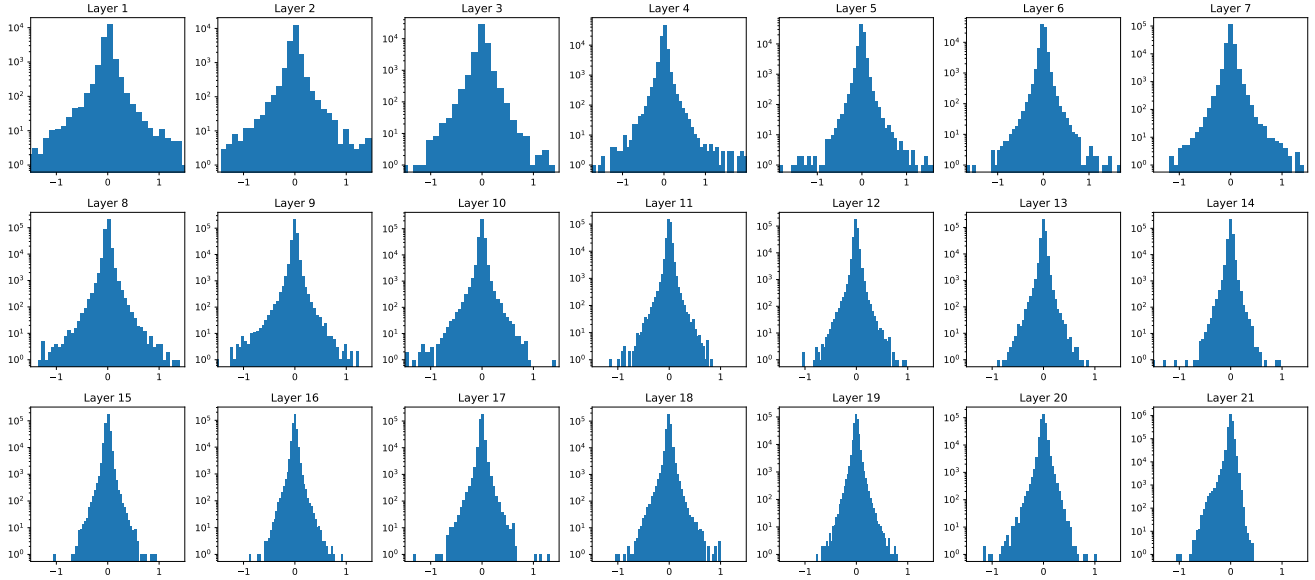


(a) RepVGG-A0 Conv  $3 \times 3$

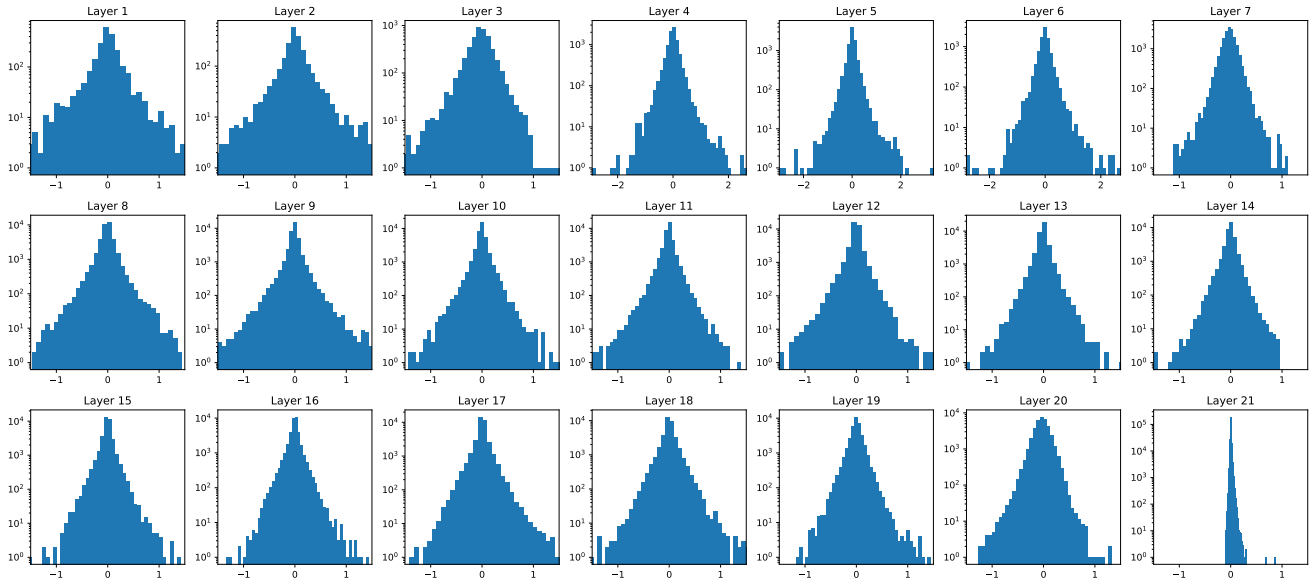


(b) RepVGG-A0 Conv  $1 \times 1$

Figure 15. Weight distribution in each layer of RepVGG-A0 trained without custom  $L_2$  regularization.



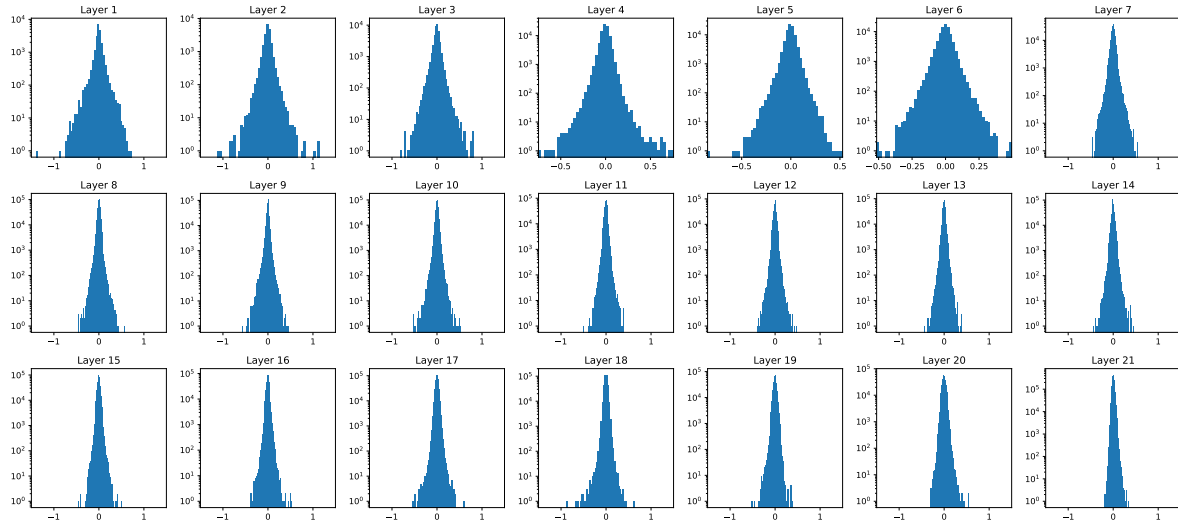
(a) RepVGG-A0 Conv  $3 \times 3$



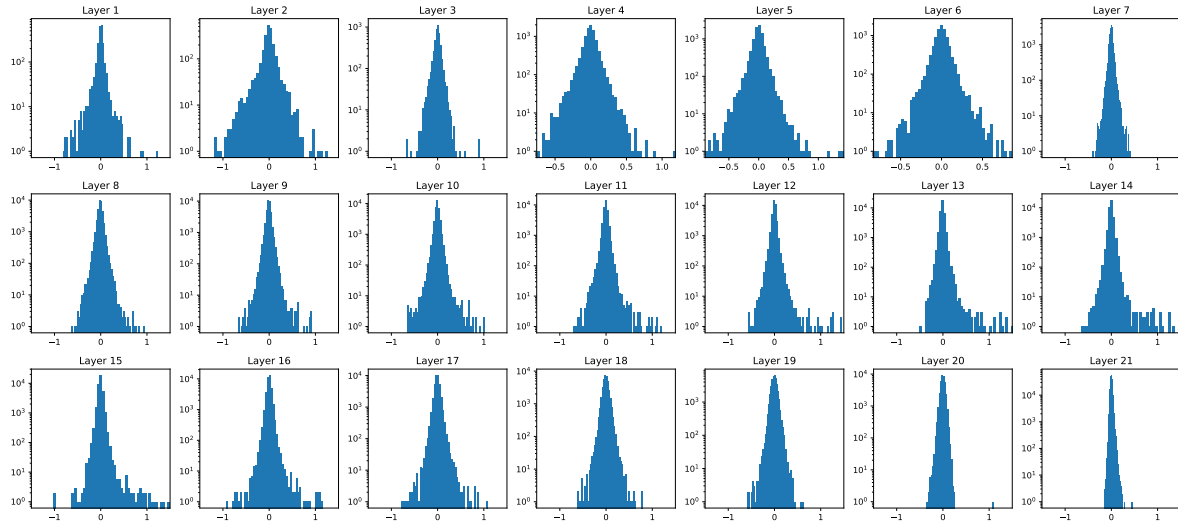
(b) RepVGG-A0 Conv  $1 \times 1$

Figure 16. Weight distribution in each layer of RepVGG-A0 trained when removing  $\gamma/\sqrt{\sigma^2 + \epsilon}$  in custom  $L_2$  regularization.

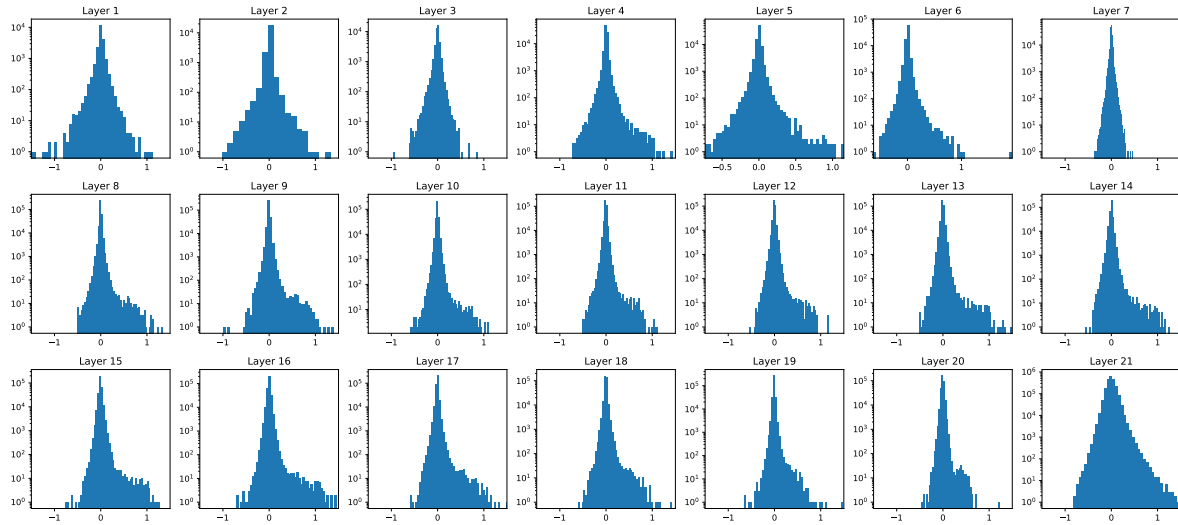




(a) QARepVGG-A0 Conv  $3 \times 3$



(b) QARepVGG-A0 Conv  $1 \times 1$



(c) Fused QARepVGG-A0

Figure 17. Weight distribution of Conv  $3 \times 3$  and  $1 \times 1$  and fused Conv in each layer of QARepVGG-A0.